Int J Adv Manuf Technol (2013) 68:1949–1965
DOI 10.1007/s00170-013-4800-9

ORIGINAL ARTICLE

Metal flow characteristics of local loading forming process for rib-web component with unequal-thickness billet

Da-Wei Zhang · He Yang

Received: 19 July 2012 / Accepted: 24 January 2013 / Published online: 8 February 2013

Abstract To explore the metal flow and filling law of large-scale rib-web component local loading forming process is important for fast design of unequal-thickness billet (UTB), parameter optimization and process control of the rib-web component local loading forming process. T-shaped component forming under UTB can reflect the forming characteristics in the large-scale rib-web component forming process. In the forming process by using UTB, the width of local loading changes dynamically, the thickness difference of billet changes notably, and the boundary conditions are very complex. By introducing new assumptions, variables and boundary conditions, a mathematical model for local loading pattern caused by UTB is established by using slab method (SM). Based on the virtualizing experimental data observed by finite element method (FEM), a predicted model for the dynamic width of local loading is established by using polynomial regression and partial least squares (PLS) regression. Comparing with FEM results indicates that the relative differences are less than about 10 % for predicted model of local loading width. Comparing with FEM and physical modeling experimental results indicates that the relative differences are less than about 15 % for SM model. The metal flow, cavity fill, and increased width of local loading under local loading condition are studied by using the mathematical models and numerical simulation, and the results indicate that: the metal flow and deformation pattern under local loading are determined by the thickness of billet and the width of local loading; the increased width of local loading is determined by initial geometric parameters, and the forming parameters such as materials (Ti-6Al-4 V and Ti-6Al-2Zr-1Mo-1 V), loading speed (0.1–1.0 mm/s), temperature (950–970 °C), etc. have little influence on it; the value of x_k (position of neutral layer) under local loading pattern caused by geometric parameters of billet is less than that caused by geometric parameters of die at initial forming stage.

Keywords T-shaped component · Unequal-thickness billet · Local loading · Slab method · Finite element method · Metal flow

D.-W. Zhang (✉) · H. Yang
School of Materials Science and Engineering,
Northwestern Polytechnical University,
127 You Yi West Rd., P.O. Box 542,
Xi'an, Shaanxi 710072,
People's Republic of China
e-mail: zhangdawei2000@yahoo.com.cn

D.-W. Zhang
e-mail: zhangdawei2000@mail.xjtu.edu.cn

D.-W. Zhang
School of Mechanical Engineering, Xi'an Jiaotong University,
Xi'an 710049, People's Republic of China

1 Introduction

The large-scale integral complex rib-web components of titanium alloy have been widely used in aviation and aerospace industries because of its high performance and lightweight [1, 2]. Isothermal local loading process, which is an isothermal die forging process by introducing local loading method, can decrease forming load and control metal flow, and thus the challenges to form these components such as large forming load and difficulty of controlling forming quality can be solved by isothermal local loading method. Thus, isothermal local loading forming technology provides a new feasible approach for plastic forming of the large-scale complex components of hard-to-deform materials [2–4]. An intermittent local loading method is that upper die or lower die is divided into several parts and only partial die is loaded in one local loading step [4, 5]. For large-scale rib-web component, this local loading method is a simple and efficient way to decrease the deformed area and enlarge forming size.

However, to avoid under-filling defect in local loading process of large-scale complex rib-web component is one of the key problems in industrial application. The large-scale rib-web component not only has large geometric size and complex-shaped structure but also has an extreme size characteristic. For example, one rib-web component (which is presented in the study [6]) shown in Fig. 1, the length is greater than 1,300 mm, and the width is about 1000 mm, but the width of most ribs is only 13 mm. So the metal is difficult to flow over the formed rib from one region to another. And the flowing over the formed rib will result in folding/lap defect [7]. In order to solve the difficulty of cavity fill and avoid occurrence of folding defect, the billet should have a proper geometry for sufficient cavity fill and appropriate metal flow [7, 8]. The cavity fill in the manufacturing process of large-scale rib-web titanium alloy component can be efficiently improved by using simple unequal-thickness billet (thickness of billet is changed by using simple step structure) combining local loading with low cost and short cycle. Zhang et al. [9] reported that simple unequal-thickness billet (UTB) has been used in industrial forming process of a TA15 (Ti-6Al-2Zr-1Mo-1 V) titanium alloy bulkhead, and a prospective cavity fill was obtained and no folding defect was observed. In Refs. [10, 11], the component was divided into two portions (the easy forming region and difficult forming region), and the thickness of different regions were designed according to the volume of the component in different portions. The cavity fill can be improved by using this UTB, but there also exists notable under-filling in some regions. Only the proper UTB is able to control the forming process and to improve cavity fill efficiently. It is necessary to explore metal flow and filling law of local loading process with UTB.

The local loading patterns in local loading process of rib-web component are determined by geometric parameters of die (GPD) and geometric parameters of billet (GPB) respectively. Under the local loading pattern caused by GPD, the width (l) of local loading is a constant, and the relation between stroke of upper die and thickness of billet in loading area is linearly dependent. In the study [6], local loading with equal-thickness billet (ETB) for T-shaped component was designed, which can reflect local loading forming characteristic caused by GPD, and a simplified slab method (SM) model was established to quickly predict metal flow and cavity fill in the process. However, under the local loading pattern caused by GPB (i.e., caused by UTB), there exists thickness difference (ΔH) due to adopting UTB. The width of local loading is dynamically changing, and the relation between stroke of upper die and thickness of billet in loading area is nonlinearly dependent. Not only is the boundary condition different, but also a new variable such as thickness difference appears. The model in the study [6] is not suitable to describe the metal flow and filling law under the local loading pattern caused by GPB. Thus, it urgently needs to explore the local loading characteristic and to understand metal flow and filling law of local loading process with UTB.

For the forming process of large-scale complex component, it is difficult to quickly obtain basic forming law and to quickly understand generic deformation characteristic because of large geometric size, complex shape, multiplicity of associated processing parameters, and mass processing data. Exploring the basic law of forming process can be carried out by considering planes of metal flow, investigating the typical position selected from the whole component. For example, Shan et al. [3] selected two typical positions

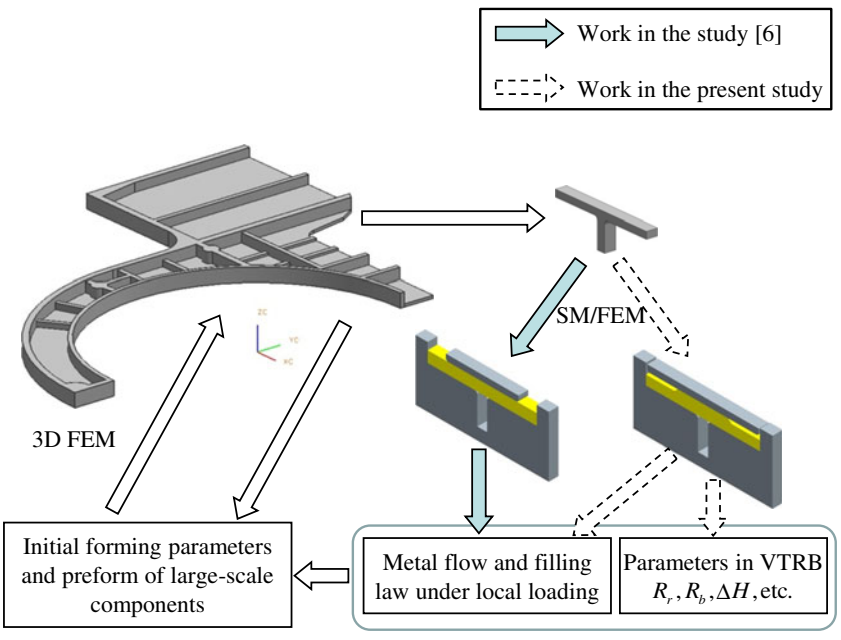

Fig. 1 Process analysis route with time-saving for large-scale rib-web component

from hatch (500 mm in length and 400 mm in width) with cross ribs on one side in order to investigate the local loading process. A basic three-dimensional preform for an asymmetric rib-web component (49 mm in length and 35 mm in width) was designed according to analysis on three cross sections [12]. As mentioned above, the large-scale rib-web component has large geometric size and its isothermal local loading process is very complicated, so putting forward and designing the eigenstructure which can reflect generic forming characteristic is the key to understand local loading characteristics in the process. Analyzing the structural characteristic of the large-scale rib-web component, it can be found this component may be considered as a combination of many T-shaped components. Local loading for T-shaped component can describe the local loading forming characteristics of rib-web component forming process. Thus, a time-saving route for process optimization as shown in Fig. 1 can be carried out.

Thus, based on the local loading for T-shaped component presented in the study [6], and through altering the thickness distribution and boundary condition, the forming process is designed to reflect the metal flow characteristics under the local loading pattern (where width of local loading is dynamically changing). T-shaped component forming process with UTB is analyzed by using SM and finite element method (FEM). By introducing the new assumptions, variables and boundary conditions, a SM model is established to describe the local loading pattern caused by GPB. The virtualizing orthogonal experimental results observed by FEM are taken as sample data, a predicted model for the dynamic width of local loading is established by using polynomial regression and partial least squares (PLS) regression. The metal flow, cavity fill, and increased width of local loading under local loading condition are studied by using the mathematical models. The forming characteristic under local loading pattern caused by GPB is compared with that caused by GPD. The comparison of rib height in multi-rib local loading process between SM and FEM results is also carried out. The results in the present study are significant for fast design of UTB, parameter optimization and process control of the large-scale rib-web component local loading forming process.

2 Local loading process and research method

2.1 Description of local loading pattern

Isothermal local loading process is an isothermal die forging process at low loading speed by local loading method, which can decrease forming load, control metal flow, improve forming quality, enlarge size range of formed component and enlarge the capability of current equipment. In the present study, the local loading method is realized by dividing upper or lower die into several parts. During isothermal local loading forming process, the dies and billet are heated to the same temperature, and only partial die is loaded. In the process, there exist loading area (the area under loading partial die) and not loaded area (the area under not loaded partial die), and the not loaded area is a free boundary. At one stage, there also exists free boundary in loading area due to the geometrical structures of billet. Thus, the local loading patterns in local loading process of rib-web component are caused by GPD and GPB respectively. Two loading patterns are put forward and designed, which could reflect the local loading characteristic of large-scale rib-web component, as shown in Fig. 2.

Under local loading pattern caused by GPD, the width of local loading does not change in the process, and the relation between stroke of upper die and thickness of billet in loading area is linearly dependent. However, under local loading pattern caused by GPB, the width of local loading changes dynamically, and the relation between stroke and thickness of billet in loading area is nonlinearly dependent. The SM model established in the study [6] can be used to describe the local loading pattern caused by GPD. But for local

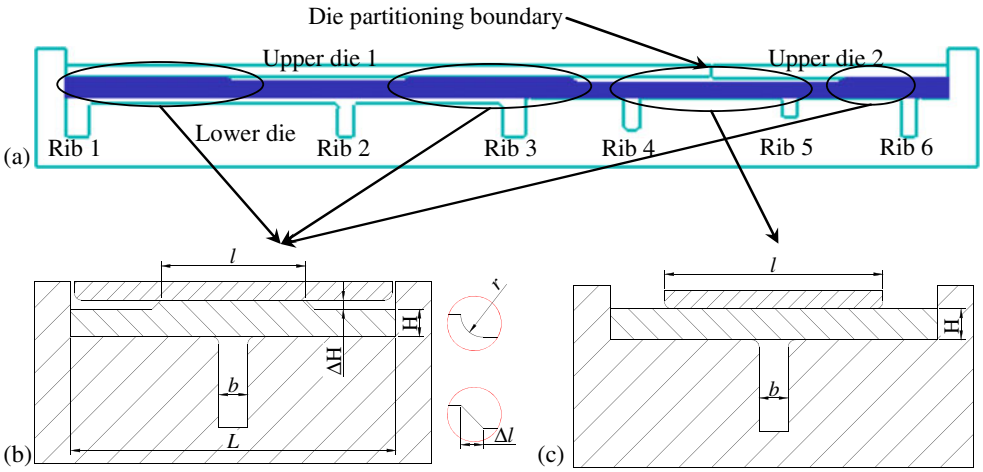

Fig. 2 Sketch of local loading processes of multi-ribs and T-shaped components: **a** multi-rib component; T-shaped component reflects the local loading forming characteristic caused by **b** GPB, **c** GPD

loading pattern caused by DPB, it not only needs to alter the boundary conditions but also needs to introduce new assumptions and variables.

The present study is concerned chiefly with the study of metal flow characteristic in the process by using UTB. The research of finite element simulation indicates [13] that the variable-thickness region of billet (VTRB) should set at web position and the transition of VTRB should choose rounding or beveling pattern. In general, the transition condition are $R_r=r/\Delta H=1.0$ (for rounding pattern) and $R_b=\Delta l/\Delta H>1.0$ (for beveling pattern). Thus, only the VTRB at web position is discussed in the present study, and the rounding and beveling patterns are adopted. Considering the restricted effects of other deformed region in the process, the T-shaped component local loading under UTB shown in Fig. 2b is put forward and designed to investigate the metal flow characteristics in the process with UTB.

2.2 Research method

2.2.1 Slab method

The slab method, which is known as the free-body equilibrium approach, is a classical approach for analyzing metal forming processes, and the mathematical model based on the SM has a clear physical insight, and its computation is simple and time efficient [14–16]. In SM analysis, a slab element with infinitesimal thickness is selected perpendicular to the direction of metal flow; and a differential equation is obtained according to force balance; and then integrating over the deformation zone and taking into account the boundary conditions, the stress distribution and the forces can be approximately calculated[17, 18].

In the isothermal forming process of titanium alloy at low loading speed, the assumptions and simplifications of the SM approached to true process conditions [18]. Some key assumptions and treatments have been made according to basic assumptions of classical slab method and isothermal forming characteristics of large-scale rib-web components: the die is considered as a rigid body, and the billet as a rigid-plastic material; the plastic deformation is by plane strain, and the volume is invariable in the process; the change of temperature is neglected, and the flow stress is considered as constant in the deformation region; the planes perpendicular to the metal flow direction define principal plane, and the principal stresses do not vary on these planes; the shear surface in neighborhood of cavity is simplified as a vertical line; the shear friction model is employed to describe the friction at die-billet interface.

O'Connell et al. [19] presented the metal flow is restricted by the die wall in closed-die upsetting process and proposed a modification to the traditional SM to reduce deformation zone when applying SM to analyze closed-die upsetting. There exists similar deformation characteristic in the process shown in Fig. 2b. The billet/workpiece can be divided into two distinct layers of similar deformation characteristic as shown in Fig. 3. In time dt, layer 2 is considered to undergo rigid-body motion.

2.2.2 Finite element method

The finite element model for isothermal forming process of T-shaped component shown in Fig. 2b is built through DEFORM package. The thermal events in the process are neglected, and the Von Mises yielding criteria and shear friction model are employed. The local refined meshing and automatic remeshing techniques are used to avoid meshing-induced singularity. The local mesh density in VTRB is high, as shown in Fig. 4. In the study [6], the comparison of rib height between experiment and FEM indicated that the error is less than 10 %. In the present study, FEM results in the process with UTB are compared with experimental ones to further validate the finite element model, which is discussed in Section 5.3.

Thus, based on the validated finite element model, the FEM results in the present study can be considered to be valid. In Sections 3.2, 4, and 5.1, the Ti-6Al-4 V titanium alloy is used in finite element analysis (FEA), and its flow

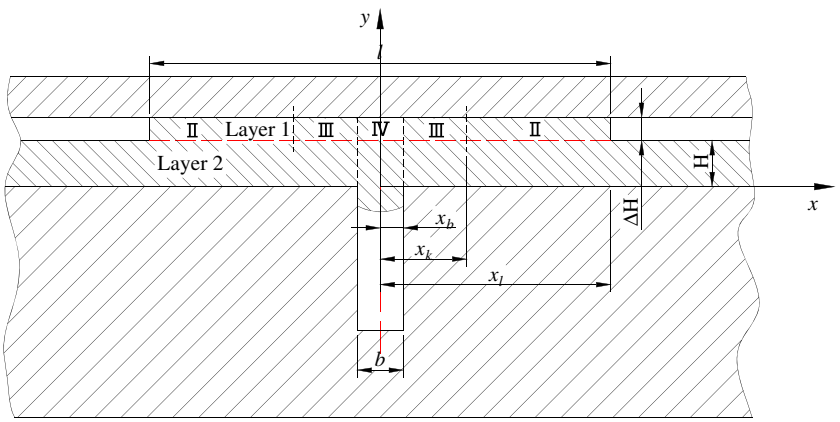

Fig. 3 Dividing the billet/workpiece into layers for modified SM analysis

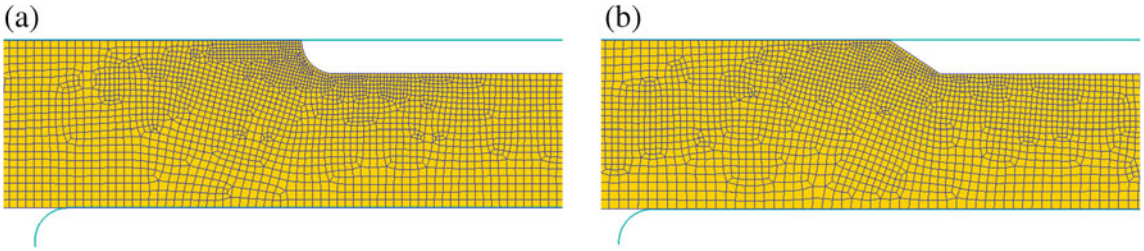

Fig. 4 Local refined meshes for variable-thickness region: **a** rounding transition pattern and **b** beveling transition pattern

behavior comes from the material library of DEFORM; the forming temperature 950 °C and loading speed v=1 mm/s are adopted; the friction factor m=0.3 is chosen according to recommending for hot forming of titanium alloy with glass lubricant [17].

2.2.3 Physical modeling experiment

It is necessary to perform the relevant experiments in order to validate the analytical and numerical analyses. The present study is concerned chiefly with the study on the forming process of titanium alloy under low strain rate and high temperature (isothermal forming). The material of the die is a nickel-base superalloy. The titanium alloy and nickel-base superalloy are relatively expensive, and the experiment needs long time and high-performance equipment. In order to simplify the experiment, reduce the cost and save the time, the experiment research is carried out by means of physical modeling of real titanium alloy forming process. Lead can be selected as modeling material for titanium alloy hot forming. Zhang et al. [6] presented that the distribution of strain in the local loading process (at room temperature) using lead is similar to the distribution of strain in the local loading process (at elevated temperature) using Ti-6Al-4 V titanium alloy. The forming process as shown in Fig. 2b is carried out on electronic universal testing machine. The lead is selected as formed material. The dies used in experiment are shown in Fig. 5, which consist of upper die and splitsegment lower die. Under the same conditions, the SM and FEM analyses are also carried out, and the main parameters are listed in Table 1.

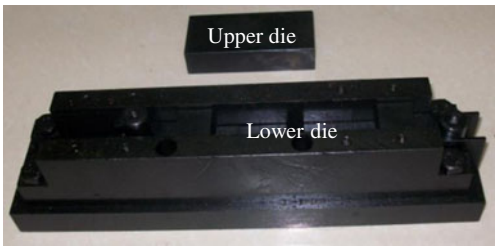

Fig. 5 Dies used for forming process of T-shaped component

3 Analysis of forming process under local loading pattern caused by GPB

3.1 SM analysis

By introducing new assumptions, variables and boundary conditions, the SM analysis which is similar to that in the study [6] can be carried out for local loading pattern caused by GPB. The deformation in layer 1 shown in Fig. 3 is similar to the deformation in the T-shaped local loading process in the study [6], but the boundary condition for region II is different. There exists a free boundary in region II shown in Fig. 3, so boundary condition at $x=x_l$ is

$$\sigma_x^{\mathrm{II}}\big|_{x=x_l}=0,\ \sigma_y^{\mathrm{II}}\Big|_{x=x_l}=2K \tag{1}$$

There also exist two deformation patterns named shearing deformation and upsetting-extruding deformation as declared in the study [6]. In the same way (deducing in the study [6]), the position (in positive direction of x axis) of neutral layer can be expressed as

$$x_k=\tfrac{b}{2}\quad \sigma_x^{\mathrm{II}}\big|_{x=x_b}\le q \tag{2a}$$

$$x_k=\tfrac{1}{4}(l+b)-\tfrac{\Delta H}{2m}\left(1+\tfrac{H+\Delta H}{2b}\right)\quad \sigma_x^{\mathrm{II}}\big|_{x=x_b}>q \tag{2b}$$

where

$$\sigma_x^{\mathrm{II}}\big|_{x=x_b}=\sigma_y^{\mathrm{II}}\Big|_{x=x_b}-2K=\frac{mK}{\Delta H}(l-b) \tag{3}$$

$$q=\frac{1}{H+\Delta H}\int_0^{H+\Delta H}\sigma_x^{\mathrm{IV}}dy=2K\left(1+\frac{H+\Delta H}{2b}\right) \tag{4}$$

Here, b is the rib width, l is the width of local loading, ΔH is the thickness difference of VTRB, H is the thickness of layer 2, i.e. the thickness of billet between VTRB and vertical wall of lower die, as shown in Fig. 2b; and m is shear friction factor.

The neutral layer is within the material of layer 1 giving inward and outward flow. The rib cavity is filled by the metal flowing inward (metal in region III and IV). The l is

Table 1 Parameters in physical modeling experiment

	Experiment	FEM	SM
Material of billet	Lead	Lead [a]	–
Temperature of billet T/°C	Room temperature	20	–
Friction factor m	Lubricating	0.3	0.3
Speed of upper die v/mm s^{-1}	–	1	–
Rib width b/mm	8	8	8
l_0/mm	40, 52	40, 52	40, 52
L/mm	90	90	90
H_0/mm	8	8	8
ΔH_0/mm	4	4	4
R_b	2	2	2

[a] $\sigma=30.20826\varepsilon^{0.11847}$(MPa)

lengthened by some of the metal flowing outward (metal in region II), and H is thickened by the other. Thus, the ΔH is a function of H and stroke s, which can be expressed as follows:

$$\Delta H = C_1 - s - H, \mathrm{d}(\Delta H) = -\mathrm{d}s - \mathrm{d}H \tag{5}$$

where C_1=H_0+ΔH_0, H_0 and the ΔH_0 is the initial values before loading.

The increased width (δ) of local loading can be expressed as second-order polynomial according to the analysis in Section 3.2, and the constant coefficient, first-order coefficient and second-order coefficient are expressed as a, b_1, and b_2 respectively. The study in Section 4 indicates that the absolute value of the constant coefficient a is much less than initial value (l_0) of l. Thus, the width of local loading can be expressed as follows:

$$l = l_0 + \delta \approx l_0 + b_1 s + b_2 s^2 \tag{6}$$

In time dt, stroke of upper die is ds. In positive direction of x axis, the volume (dV_{in}) of metal flowing inward and the volume (dV_{out}) of metal flowing outward can be expressed as Eqs. (7) and (8) according to the volume constancy principle.

$$\mathrm{d}V_{\mathrm{in}} = x_k \cdot \mathrm{d}s \tag{7}$$

$$\mathrm{d}V_{\mathrm{out}} = \left(\frac{l}{2} - x_k\right) \cdot \mathrm{d}s \tag{8}$$

The warping or haunch-up in not contacted area (i.e. the area between VTRB and vertical wall of lower die) is neglected, and the thickening of H is supposed to be homogeneous. Thus, layer 2 is thickened by dH and layer 1 is thickened by d(ΔH) in time dt, and the dV_{out} can be expressed as Eq. (9) according to the volume constancy principle, where d(ΔH) is a negative according to Eq. (5).

$$\mathrm{d}V_{\mathrm{out}} = (\Delta H + \mathrm{d}(\Delta H))\frac{\mathrm{d}l}{2} + \frac{L-l}{2}\mathrm{d}H \tag{9}$$

According to Eqs. (2) and (5)–(9), and neglecting second-order terms, and letting

$$K_1 = L - l_0,$$

$$K_2 = -b_1 C_1 - b + l_0,$$

$$K_3 = -2(b_2 C_1 - b_1),$$

$$K_4 = b_1 - \frac{1}{m} - \frac{C_1}{2mb},$$

$$K_5 = 2b_2 + \frac{1}{2mb},$$

$$K_6 = -C_1 K_4 + \frac{1}{2}(l_0 - b),$$

$$K_7 = \frac{b_1}{2} + K_4 - C_1 K_5,$$

$$K_8 = K_5 + \frac{b_2}{2},$$

then there exist differential equations Eq. (10) in shearing deformation $\left(\sigma_x^{\mathrm{II}}\big|_{x=x_b} \le q\right)$,

$$\begin{cases} (K_1 - b_1 s - b_2 s^2)\frac{\mathrm{d}H}{\mathrm{d}s} - (b_1 + 2b_2 s)H = K_2 + K_3 s + 3b_2 s^2 \\ \frac{\mathrm{d}V_{\mathrm{in}}}{\mathrm{d}s} = \frac{b}{2} \end{cases} \tag{10}$$

and there exist differential equations Eq. (11) in upsetting-extruding deformation $\left(\sigma_x^{\mathrm{II}}\big|_{x=x_b} > q\right)$.

$$\begin{cases} (K_1 - b_1 s - b_2 s^2)\frac{dH}{ds} - (K_4 + K_5 s)H = K_6 + K_7 s + K_8 s^2 \\ \frac{dV_{in}}{ds} = \frac{1}{4}(l_0 + b + b_1 s + b_2 s^2) - \frac{C_1 - s - H}{2m}\left(1 + \frac{C_1 - s}{2b}\right) \end{cases} \tag{11}$$

Substituting Eqs. (3) and (4) into $\sigma_x^{II}\big|_{x=x_b} > q$, the following expression can be obtained.

$$\Delta H(2b + H + \Delta H) < mb(l - b) \tag{12}$$

q is a decreasing function of s according to Eqs. (4) and (5); and $\sigma_x^{II}\big|_{x=x_b}$ is a increasing function of s according to Eqs.(3), (5) and (6). Thus, if friction factor m and initial values of geometric parameters satisfy the Eq. (12), then the deformation is upsetting-extruding deformation at all the local loading stage. In other words, $\sigma_x^{II}\big|_{x=x_b} > q$ at all the local loading stage, and then the differential equations Eq. (11) can be solved based on the initial value condition Eq. (13).

$$H|_{s=0} = H_0, V_{in}|_{s=0} = 0 \tag{13}$$

If friction factor m and initial values of geometric parameters do not satisfy Eq. (12), then there exists a critical stroke s_k which makes $\sigma_x^{II}\big|_{x=x_b} = q$. If $s \le s_k$, then $\sigma_x^{II}\big|_{x=x_b} \le q$, and the initial value condition for differential equations Eq. (10) is Eq. (13); if $s > s_k$, then $\sigma_x^{II}\big|_{x=x_b} > q$, and the initial value condition for differential equations Eq. (11) is Eq. (14).

$$H|_{s=s_k} = H_k, V_{in}|_{s=s_k} = \frac{b}{2}s_k \tag{14}$$

3.2 FEM analysis

The forming load and δ in the T-shaped component forming process using UTB are shown in Fig. 6. The forming process can be divided into three stages according to the contact state of billet with dies.

The first stage, with which the present study is concerned chiefly, has a notable local loading characteristic, and only partial billet contacts with upper and lower dies, and thus the increase in load is little.

At the second stage, a V-shaped cavum occurs between VTRB and upper die, and then the cavum will disappear or form folding/lap[1]; and local loading characteristic turns into whole loading characteristic gradually, and thus the load increase sharply.

The third stage has a notable whole loading characteristic, and load curve is smooth.

The FEM results indicate the ΔH decreases and H increases at the first stage (i.e., local loading stage). Of course, the thickening of H is inhomogeneous. The increased widths of local loading under rounding and beveling patterns are

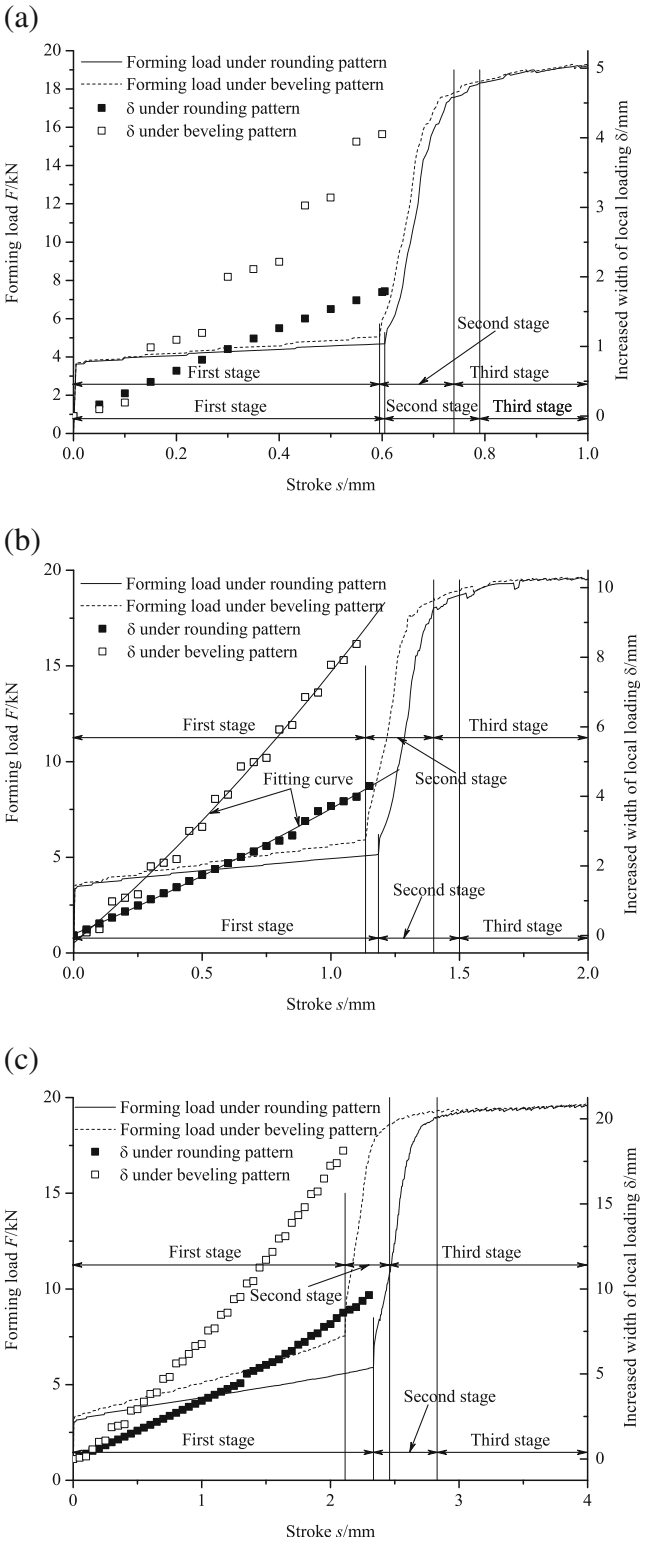

Fig. 6 Forming load and increased width of local loading under various thickness differences: **a** $\Delta H_0/H_0$=0.125; **b** $\Delta H_0/H_0$=0.250; and **c** $\Delta H_0/H_0$=0.500

[1] The forming defect is not discussed in the present study. The detailed discussion about the forming conditions of the V-shaped cavum to be planished or to form folding can be found in the study [13].

expressed as δ_r and δ_b respectively. It can be seen from Fig. 6 that the increasing speed of δ_b is greater than the increasing speed of δ_r. In VTRB, distance between point in transition region and upper die under beveling pattern is less that under rounding pattern, and thus the beveling pattern is suitable for forming new contact area. But the rounding pattern is smooth and the change of increased widths (δ) is also smooth, especially at initial stage.

It can be found that increased widths of local loading can be expressed as second-order polynomial through observing the variation of sample data shown in Fig. 6. The increasing width is a function of stroke, and it can be expressed as follows:

$$\delta = f(s) = a + b_1 s + b_2 s^2 \tag{15}$$

The factor s is in unit of millimeter. The polynomial regression can be carried out based on the sample data shown in Fig. 6b, and regression equations of δ_r and $\delta_b$can be expressed as follows:

$$\delta_r = f_r(s) = 0.04065 + 3.09134s + 0.51204s^2 \tag{16a}$$

$$\delta_b = f_b(s) = -0.21783 + 6.31209s + 1.47036s^2 \tag{16b}$$

The variance analysis (F test) shown in Table 2 indicates that the established polynomial regression equations are significant. It can be seen from Eq. (16) and Table 3 that constant coefficient (a) of polynomial regression equation is small, and has little influence. In general, the absolute value of a under beveling is greater than that under rounding, because change of increased widths smooth at initial stage under rounding pattern. The δ in local loading process can be predicted by using polynomial regression equation, and the l in the process can be described by Eq. (6).

4 Predicted model for dynamic width of local loading

The width of local loading is a key local loading condition and plays an important role on metal flow, cavity fill and deformation behavior. The width of local loading is dynamically changing in the process with UTB. Thus, prediction for increased width δ is a key to establish the predicted model of the width l under local loading pattern caused by GPB. The δ can be expressed as a second-order polynomial according to the analysis in Section 3.2, but the initial geometric parameters such as l_0, L, H_0, etc. affect the values of polynomial regression coefficients such as a, b_1, and b_2.

4.1 Experiment design and sample data

The sample data of δ in local loading stage is obtained by the virtualizing experiments which are carried out by FEM simulation. According to the design criterion about rib-web component of titanium alloy in the relevant handbook and the size of one large-scale rib-web component of titanium alloy, at the same time, the initial values of geometric parameters should reduce the shearing deformation time and satisfy the suggestions about R_r and R_b , the range of initial geometric parameters is determined as follows:

$$\begin{aligned}
&l_0/b = 5 - 20;\\
&L/l_0 = 1.5 - 10.0, L < 1000\text{mm};\\
&H_0/b = 0.75 - 2.25, H_0 < \sqrt{mb(l_0 - b)};\\
&\Delta H_0/H_0 = 0.125 - 1.000;\\
&R_r = 1;\\
&R_b = 1 - 4(R_b \cdot \Delta H_0 < (L - l_0)/2).
\end{aligned}$$

Millimeter is used as unit for the above parameters such as l_0, b, L, H_0, ΔH_0. The orthogonal experiment design array $L_{25}(5^6)$ is adopted, which are carried out by FEM simulation. For rounding pattern, four factors, which are A (l_0/b), B (L/l_0), C (H_0/b) and D ($\Delta H_0/H_0$), and five levels are designed in the array; but for beveling pattern, five factors, which are A (l_0/b), B (L/l_0), C (H_0/b), D ($\Delta H_0/H_0$) and E (R_b), and five levels are designed in the array. When the value of one geometric parameter exceeds the above limitation, then the experiment is removed from the array. The sample data under different initial geometric parameters are obtained according to FEM results. The second-order polynomial equations of δ=f(s) are built based on the obtained data. The final virtualizing experiment design array and the results (a, b_1, and b_2) are listed in Table 3.

4.2 PLS regression modeling

PLS regression method is used to analyze the data listed in Table 3 due to the multi response variables and few test number. PLS regression is a recently developed generalization

Table 2 Variance analysis

Source	Variation *SS*		Degree of freedom *df*		Variance *MS*		Variance ration *F*		$F_{0.01}(2,21)$	$F_{0.01}(2,20)$
	Rounding pattern	Beveling pattern	Rounding pattern	Beveling pattern	Rounding pattern	Beveling pattern	Rounding pattern	Beveling pattern	Rounding pattern	Beveling pattern
Regression	39.010	159.557	2	2	19.505	79.778	4729.888	1883.790	5.78	5.85
Error	0.087	0.847	21	20	0.004	0.042				
Total	39.097	160.404	23	22						

of multiple linear regression [20]. It can analyze data with strongly multi-collinear, small sample size, and numerous predictor variables, and also simultaneously model several response variables [20, 21]. The literatures [20, 21] presented the details about PLS regression method.

The predictor variables **X** and response variables **Y** are expressed as $X=(x_1,x_2, x_p)_{n\times p}$ [2] and $Y=(y_1,y_2, y_q)_{n\times q}$ respectively. Using the PLS regression method the regression equation Eq. (17) can be obtained.

$$\mathbf{Y} = \mathbf{XB} \tag{17}$$

where **B** is the matrix of regression coefficients, whose size is $p\times q$ in general. But the matrix **B** includes the constant coefficient in the present study, whose size is $(p+1)\times q$. And the regression coefficients vector of the ith y is

$$\mathbf{b}_i = \left(a_{i0}, a_{i1}, a_{i2}, \cdots, a_{ip}\right)^{\mathrm{T}} \tag{18}$$

Where a_{i0} is the constant coefficient.

Under rounding pattern, the relationships between initial geometric parameters and the coefficients (a,b_1, b_2) are not a simple linear. A fine model such as Eq. (19a) is built according to the analysis and the experiential knowledge.

$$\begin{cases} a = \ln(a_0 + a_1A + a_2B + a_3C + a_4D) \\ b_1 = e^{a_0}A^{a_1}B^{a_2}e^{a_3C}e^{a_4D} \\ e^{b_2} = e^{a_0}A^{a_1}B^{a_2}C^{a_3}D^{a_4}e^{a_5AB}e^{a_6AC}e^{a_7AD}e^{a_8BC}e^{a_9BD}e^{a_{10}CD} \end{cases} \tag{19a}$$

The Eq. (19a) is linearized as follows:

$$\begin{cases} e^a = a_0 + a_1A + a_2B + a_3C + a_4D \\ \ln b_1 = a_0 + a_1\ln A + a_2\ln B + a_3C + a_4D \\ b_2 = a_0 + a_1\ln A + a_2\ln B + a_3\ln C + a_4\ln D + a_5AB + a_6AC + a_7AD + a_8BC + a_9BD + a_{10}CD \end{cases} \tag{19b}$$

Three times of simple PLS regression are carried out respectively, and three regression coefficients matrices whose sizes are 5×1, 5×1 and 11×1 are obtained. They are combined into one matrix as follows:

$$\mathbf{B}_r = \begin{pmatrix} 0.96069 & 0.01071 & 0.98615 \\ -0.00756 & 1.06763 & 0.12678 \\ 0.00776 & -0.02661 & 0.89567 \\ 0.06189 & -0.52489 & -0.13858 \\ 0.18851 & -0.39254 & 0.72958 \\ & & -0.00251 \\ & & 0.01599 \\ & & -0.02192 \\ & & -0.04845 \\ & & -0.17894 \\ & & -0.60447 \end{pmatrix} \tag{20}$$

where $\mathbf{b}_{r1}$ is the regression coefficients vector of a, whose size is 5×1; $\mathbf{b}_{r2}$ is the regression coefficients vector of b_1, whose size is 5×1; $\mathbf{b}_{r3}$ is the regression coefficients vector of b_2, whose size is 11×1.

Under beveling pattern, the relationships between initial geometric parameters and the coefficients (a,b_1, b_2) are not a simple linear. A fine model such as Eq. (21a) is built according to the analysis and the experiential knowledge.

$$\begin{cases} e^a = e^{a_0}A^{a_1}B^{a_2}e^{a_3C}e^{a_4D}E^{a_5} \\ b_{1,2} = e^{a_0}e^{a_1A}e^{a_2B}e^{a_3C}e^{a_4D}e^{a_5E}A^{a_6}B^{a_7}C^{a_8}E^{a_9} \end{cases} \tag{21a}$$

The Eq. (21a) is linearized as follows:

$$\begin{cases} a = a_0 + a_1\ln A + a_2\ln B + a_3C + a_4D + a_5\ln E \\ \ln b_{1,2} = a_0 + a_1A + a_2B + a_3C + a_4D + a_5E + a_6\ln A + a_7\ln B + a_8\ln C + a_9\ln E \end{cases} \tag{21b}$$

One simple PLS regression and one multivariate PLS regression are carried out respectively, and two regression coefficients matrices whose sizes are 6×1 and 10×2 are obtained. They are combined into one matrix as follows:

$$\mathbf{B}_b = \begin{pmatrix} -0.20918 & 1.16941 & -1.01970 \\ -0.50852 & 0.03880 & -0.03751 \\ 0.00006 & -0.13668 & 0.74348 \\ 1.06611 & -0.33010 & -0.04876 \\ 0.27875 & -0.47077 & -0.22359 \\ 0.10878 & -0.04376 & 1.19454 \\ & 0.17274 & 0.94165 \\ & 0.73480 & -3.74272 \\ & -0.39029 & -0.45123 \\ & 0.64892 & -1.50094 \end{pmatrix} \tag{22}$$

[2] There are p variables x_1,x_2,x_p; the n observations are carried out; and then n sample points (x_{i1},x_{i2},x_{ip}) i=1,2, n are obtained.

Table 3 Experiment design array and results

No.	$A(l_0/b)$	$B(L/l_0)$	$C(H_0/b)$	$D(\Delta H_0/H_0)$	$E(R_b)$	Rounding pattern			Beveling pattern		
						a	b_1	b_2	a	b_1	b_2
1	1(5)	1(1.5)	1(0.75)	1(0.125)	1(1.0)	0.00839	3.38577	−0.03005	−0.05568	4.48591	2.77445
2	1(5)	2(2.5)	2(1.00)	2(0.250)	2(1.5)	0.03779	3.01564	0.6396	−0.20603	5.5063	0.8235
3	2(8)	1(1.5)	2(1.00)	3(0.500)	4(3.0)	0.03027	4.86196	0.6813	0.05177	6.68939	12.76558
4	2(8)	2(2.5)	3(1.25)	4(0.750)	5(4.0)	0.11665	3.41792	0.42806	0.60275	7.03824	3.84869
5	2(8)	5(10.0)	1(0.75)	2(0.250)	3(2.0)	0.04881	5.45634	1.37873	−0.14082	8.79492	2.04758
6	3(12)	1(1.5)	3(1.25)	5(1.000)	2(1.5)	0.19034	4.64823	0.62889	0.51184	3.23136	3.83847
7	3(12)	2(2.5)	4(1.75)	1(0.125)	3(2.0)	0.02236	5.29165	0.37822	0.07937	8.66793	0.96731
8	3(12)	4(7.0)	1(0.75)	3(0.500)	5(4.0)	0.1622	7.46417	1.43687	−0.20254	18.35706	4.24518
9	3(12)	5(10.0)	2(1.00)	4(0.750)	1(1.0)	0.02393	6.22391	0.36974	−0.09424	5.59238	1.95941
10	4(16)	1(1.5)	4(1.75)	2(0.250)	5(4.0)	0.00576	7.21745	0.47883	0.31761	13.0904	14.54041
11	4(16)	3(4.0)	1(0.75)	4(0.750)	2(1.5)	0.03149	9.62553	1.16094	−0.48346	12.6891	1.15675
12	4(16)	4(7.0)	2(1.00)	5(1.000)	3(2.0)	0.26739	6.98127	0.6889	−0.63442	11.29158	1.09605
13	5(20)	1(1.5)	5(2.25)	4(0.750)	3(2.0)	0.08629	5.64025	0.37295	1.23332	3.38936	4.58819
14	5(20)	2(2.5)	1(0.75)	5(1.00)	4(3.0)	−0.06862	11.61353	0.74982	−0.917	19.96945	1.97708
15	5(20)	3(4.0)	2(1.00)	1(0.125)	5(4.0)	−0.03399	12.71566	0.66365	−0.19797	17.26508	6.21001

where $\mathbf{b}_{b1}$ is the regression coefficients vector of a, whose size is 6×1; $\mathbf{b}_{b2}$ is the regression coefficients vector of b_1, whose size is 10×1; $\mathbf{b}_{b3}$ is the regression coefficients vector of b_2, whose size is 10×1.

The plot of the X-scores ($\mathbf{t}_1/\mathbf{t}_2$) and T^2 ellipse shows the sample points are homogenous. The plot of Y (b_1 and b_2) score $\mathbf{u}_1$ vs. X-score $\mathbf{t}_1$ under beveling pattern indicates that the correlation coefficient between them is 0.91. The plot of Y (b_1) score $\mathbf{u}_1$ vs. X-score $\mathbf{t}_1$ under rounding pattern indicates that the correlation coefficient between them is 0.86. The plot of Y (b_2) score $\mathbf{u}_1$ vs. X-score $\mathbf{t}_1$ under rounding pattern indicates that the correlation coefficient between them is 0.57, where the $\mathbf{t}_1$ only captures 37.86 % of $\mathbf{X}$ and the $\mathbf{u}_1$ only captures 31.01 % of $\mathbf{Y}$. The predicted model can be composed of Eqs. (6), (15), and (19)–(22), the width l and increased width δ under local loading pattern caused by GPB can be predicted by the model.

5 Results and discussion

5.1 Evaluation of regression model

Five forming processes (examples 1–5, which differ in initial geometric parameters) are used to evaluate the predicted model established in Section 4. The evaluation is chiefly concerned with the prediction about δ.

The geometric parameters in examples 1 and 2 are symmetrical about the center of rib, based on which the sample data in Section 4 are obtained, as shown in Fig. 2b. Example 1 adopts rounding pattern, and the initial geometric parameters are l_0/b=5, L_0/l_0=2.25, H_0/b=1 and $\Delta H_0/H_0$=0.5. Example 2 adopts beveling pattern, and the initial geometric parameters are l_0/b=5, L_0/l_0=2.25, H_0/b=1, $\Delta H_0/H_0$=0.5 and R_b=2.

The transition patterns of VTRB in both sides are different in example 3, as shown in Fig. 7a: rounding pattern in region 1; and beveling pattern in region 2. The initial geometric parameters in region 1 are the same as that in example 1; and the initial geometric parameters in region 2 are the same as that in example 2.

The thicknesses of billet in both sides are different in example 4, as shown in Fig. 7b: in region 1, H_0/b=1 and $\Delta H_0/H_0$=0.5; in region 2, H_0/b=1.2 and $\Delta H_0/H_0$=0.25. Rounding pattern is adopted, and other parameters are l_0/b= 7.5 and L_0/l_0=1.5.

The widths of local loading in both sides are different in example 5, as shown in Fig. 7c: in region 1, l_0/b=5 and L_0/l_0= 2.25; in region 2, l_0/b=7.5 and L_0/l_0=2. Other parameters are H_0/b=1, $\Delta H_0/H_0$=0.5, and R_b=2.

In the case of which the initial geometric parameters are symmetrical, such as examples 1 and 2, the observed and predicted results are shown in Fig. 8a and b, and the discrepancies between predicted and observed results are less than about 10 %.

In the case of which transition patterns of VTRB are asymmetrical, such as example 3, the observed and predicted results are shown in Fig. 8c. The increased widths of local loading in region 1 and 2 are expressed as $\delta_1/2$ and $\delta_2/2$, respectively, which are predicted by Eq. (15) combining with Eq. (19) and (21). The discrepancies between predicted and observed results are less than about 5 %.

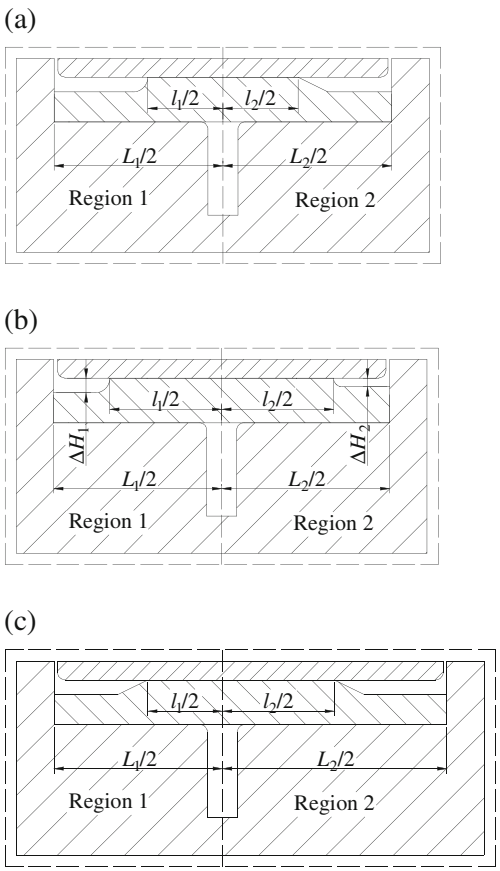

Fig. 7 Sketches of forming processes for examples 3–5: **a** example 3, **b** example 4, **c** example 5

In the case of which thicknesses of billet are asymmetrical, such as example 4, the $\delta_1/2$ in region 1 and $\delta_1/2$ in region 2 are predicted by Eq. (15) combining with Eq. (19), respectively. The observed and predicted results are shown in Fig. 8d. The times of forming stages presented in Section 3.2 in different regions have a large difference due to the difference in ΔH. The time of first stage in region 1 is almost the sum of time of first and second stages in region 2. In the time of first stage in region 2, the errors in region 1 and 2 are less than about 5 %; but in the time of second stage in region 2, the error in region 1 is less than about 10 %.

In the case of which width of local loading is asymmetrical, such as example 5, the $\delta_1/2$ in region 1 and $\delta_2/2$ in region 2 are predicted by Eq. (15) combining with Eq. (21), respectively. The observed and predicted results are shown in Fig. 8e. It can be seen from Fig. 8e that the error in region 1 is less than about 10 %, but the error in region 2 is less than about 5 %.

5.2 Influence of forming parameters on the increased width δ

Ti-6Al-4 V which is a ($\alpha+\beta$) titanium alloy is used in above study and discussion. However, another titanium alloy, TA15 (Ti-6Al-2Zr-1Mo-1 V) which is a near-alpha titanium alloy is widely used in China. In the isothermal forming process, the near-beta forging is often adopted. And the working temperature is 950 °C for conventional forging and about 970 °C for near-beta forging in industrial forming process of TA15 titanium alloy. The isothermal forging of titanium alloy is carried out under low strain rate, such as v= 0.1–1.0 mm/s in industrial forming process. The typical value of friction factor for lubricated hot forming processes is about 0.3, but the lubrication action of glass lubricant may decrease at temperatures above 950 °C under lower loading speed. For example, in the isothermal local loading forming process of one large-scale TA15 titanium alloy bulkhead (of which sizes in length and width are both greater than 1,000 mm), the forming temperature is about 970 °C, the loading speed is about 0.2 mm/s, and the friction factor m is about 0.5 determined by ring compression test [22].

The above study and discussion are based on the forming parameters such as forming material Ti-6Al-4 V, forming temperature 950 °C, friction factor 0.3 and loading speed 1 mm/s. Thus, the influences of materials (Ti-6Al-4 V and TA15), loading speeds (v=0.2 and 1.0 mm/s), forming temperatures (T=950 and 970 °C) and friction factors (0.3 and 0.5) on increased width (δ) are discussed in this section. The initial geometric parameters are the same as that in example 1 and 2 presented in Section 5.1.

It can be seen from Fig. 9 that the material has little influence on increased width under beveling pattern. Under rounding pattern, the material also has little influence on δ at initial forming stage, but there exists difference at late stage where the error between regression model and FEM is also less than about 10 %. The temperature at 950°C and 970°C has little influence on δ for TA15 titanium alloy, as shown in Fig. 10. In Fig. 10, the relative values of differences caused by temperature are about 0.4–2.5 %.

The reason for δ_b greater than δ_r is presented in Section 3.2: in VTRB, distance between point in transition region and upper die under beveling pattern is less that under rounding pattern, and thus the beveling pattern is suitable for forming new contact area. The friction and loading speed affect the metal flow near upper die, and then affect the forming of new contact area. Thus, the influences of friction (as shown in Fig. 11) and loading speed (as shown in Figs. 9–11) on δ under rounding pattern are larger than those under beveling pattern, but the change of δ is also slight. With the increase in friction at interface, the speed of metal flow outward near the interface will reduce. Thus, the δ under rounding pattern decreases with the increase in the friction. But under beveling pattern, the decreasing tendency will be reduced by forming new contact area. The speed of metal flow outward in layer 1 reduces with the decrease in loading speed, and thus the δ increases under both patterns with the increase in loading speed.

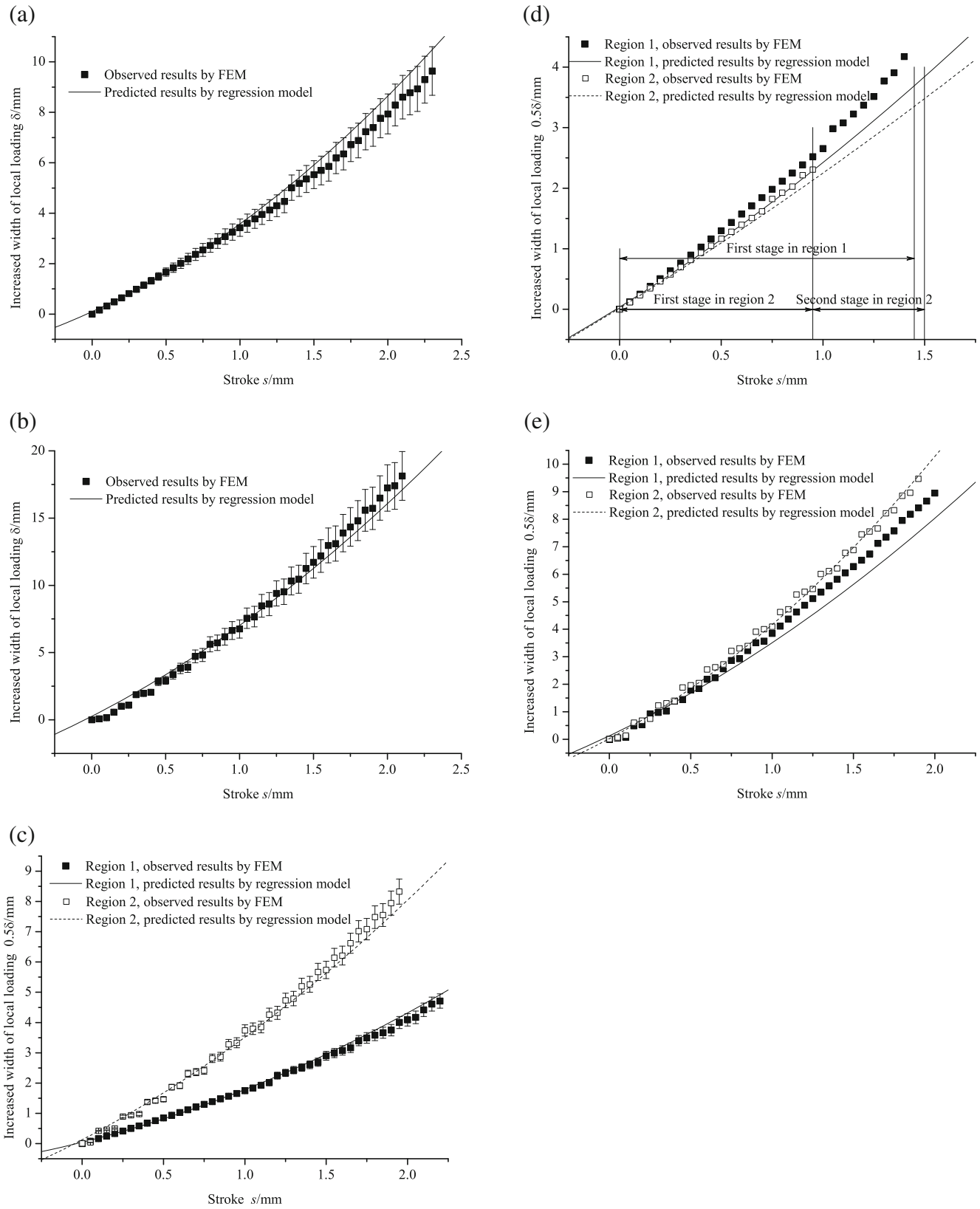

Fig. 8 Observed and predicted values: **a** example 1, **b** example 2, **c** example 3, **d** example 4, **e** example 5

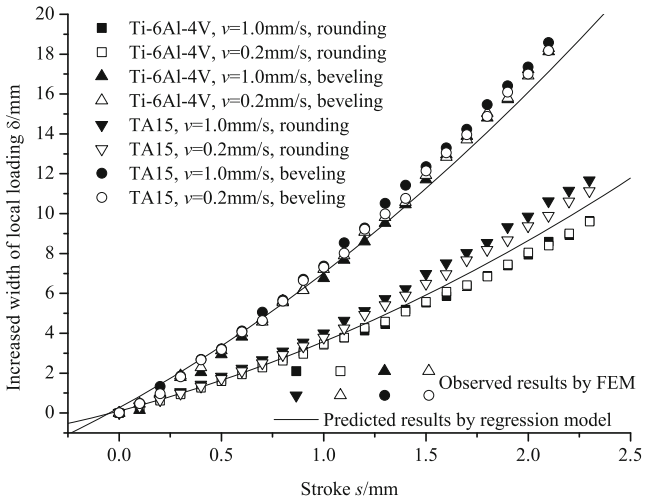

Fig. 9 Increased width of local loading for different materials (T= 950 °C, m=0.3)

5.3 Evaluation of SM model

The parameters such as position (x_k) of neutral layer, rib height (h), the thickness (H) of billet between VTRB and vertical wall, etc., would be predicted by the SM model. The H is supposed to thicken homogeneously in SM model although the thickening of H is inhomogeneous in real process. The rib height is determined by the position of neutral layer in the process. In the physical modeling experiment, the rib height is easier to measure than x_k. For the process mentioned in Section 2.2.3, the metal flowing into rib cavity can be calculated by Eqs. (10)–(14) according to the parameters listed in Table 1. The predicted model of increased width presented in Section 4 is used to predict the dynamic width of local loading, and the differential

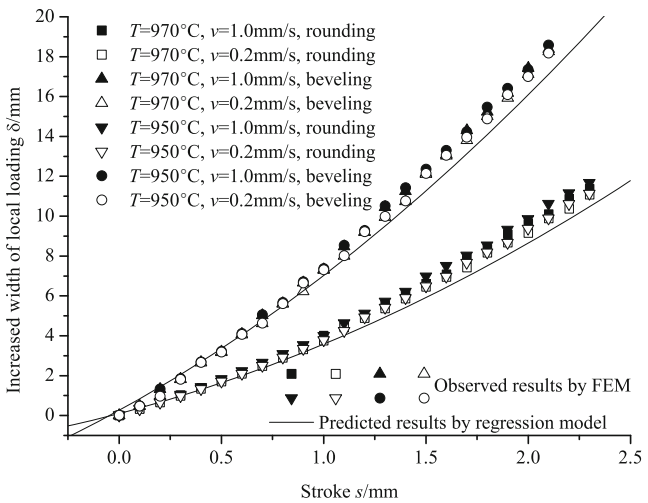

Fig. 10 Increased width of local loading under different temperatures (TA15, m=0.3)

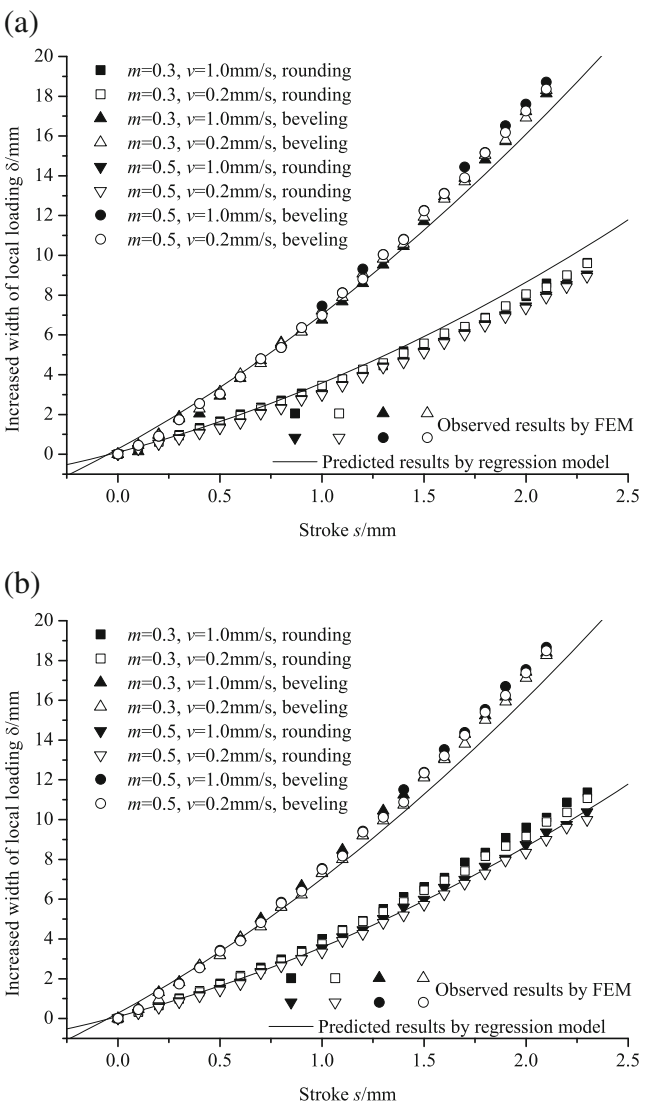

Fig. 11 Increased width of local loading under different friction factors: **a** Ti-6Al-4 V, T=950 °C; **b** TA15, T=970 °C

equations are solved by Runge–Kutta method. Thus, the comparison of rib height of SM predictions with FEM and experimental observations is carried out, as shown in Fig. 12.

It can be seen form Fig. 12 that the error between SM and experiment is less than about 15 %, and that with increasing width of local loading the SM results are closing to FEM results which is the same as that declared in the study [6]. The main reason is that simplification of shear surface in neighborhood of rib cavity brings the error which makes the SM results less than the FEM results. And the larger the l/b, the smaller the error caused by simplification of shear surface. In the FEM model, the gap between upper and lower dies and the fit clearance of splitsegment lower die are not considered. Thus, the experimental rib height is less than FEM rib height because the some metal goes to form the burr and longitudinal flash.

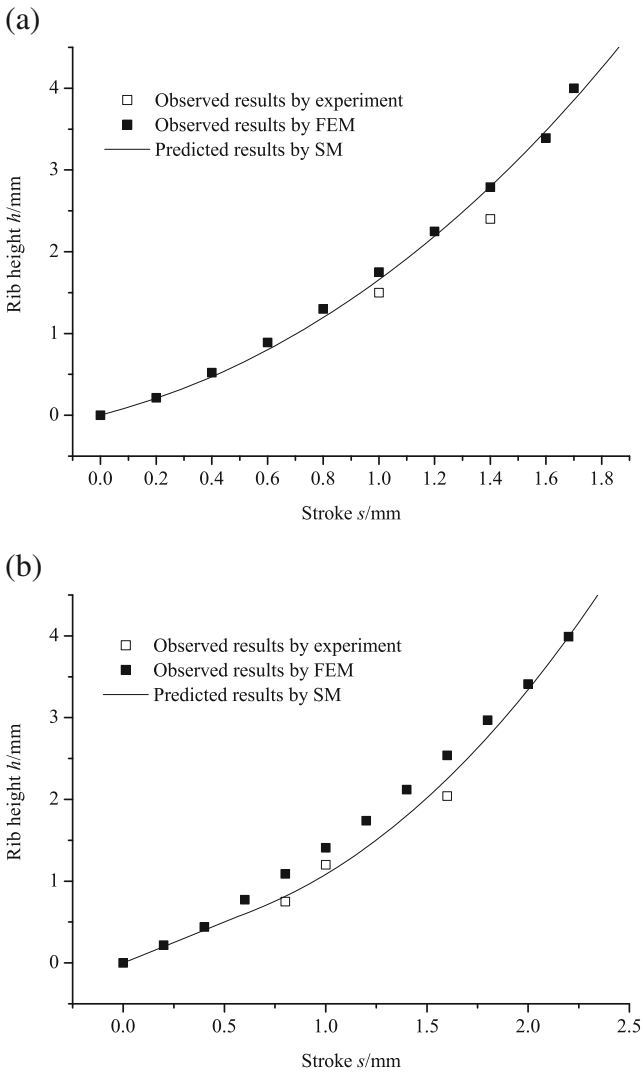

Fig. 12 Results by using different research methods: **a** l_0=52 mm; **b** l_0 =40 mm

For the condition that the geometric parameters are asymmetrical about the center of rib, such as examples 3–5 in Section 5.1, the center of rib cavity is assumed as symmetry plane for left and right regions respectively, and then the metal flowing into rib cavity in left or right region can be calculated by Eqs. (10)–(14). Then the rib height is predicted according to the total volume $\left(V_{in}^{tot}\right)$. The observed and predicted results for examples 3–5 are shown in Fig. 13 (Ti-6Al-4 V is used in FEA). The error caused by simplification of shear surface would be reduced by increasing l. Thus, it can be seen from Fig. 13 that the discrepancies between predicted and observed results are less than about 15 % for the example 3 and 10 % for the examples 4 and 5.

Under the forming conditions used in the present study, the analysis in Section 5.2 indicates that the forming parameters, such as material, temperature, loading speed and friction, have little influence on change of l. Thus, Eqs. (6) and

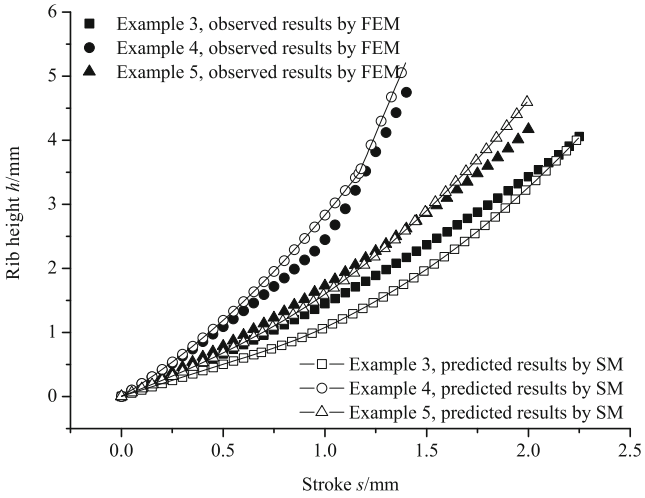

Fig. 13 Rib heights in the processes of examples 3–5

(19)–(22) can be used to predict the width of local loading under different forming parameters. Fig. 14 shows the rib height under different forming parameters, where the initial geometric parameters in Fig. 14a are the same as those in example 1 and the initial geometric parameters in Fig. 14b are the same as those in example 2. The error between SM and FEM results is less than about 15 %.

The local loading process of multi-ribs as shown in Fig.2a has two local loading steps, which is presented as following: in the first local loading step, upper die 1 is loaded whilst constraint is applied to not loaded area by upper die 2; in the second local loading step, upper die 2 is loaded and upper die 1 is fixed as constraint. In the first local loading step, the cavities of the rib 1 and 3 are filled by local loading way at initial filling stage, cavity of the rib 4 are filled by local loading way throughout the forming process. The rib height in the first local loading step can be predicted by using the SM models respectively established in the present study and the study [6]. Figure 15 shows rib heights of rib 1, 3 and 4 in local loading state. The errors between SM results and FEM data are 5–15 %.

5.4 Comparison between different local loading patterns

The SM model established in Section 3.1 can describe local loading characteristic in the process using UTB where width of local loading dynamically changes. The SM model established in the study [6] can describe local loading characteristic in the process where width of local loading does not change. The comparison of local loading characteristic between the pattern caused by GPB and the pattern caused by GPD is carried out in this section by using the SM models, respectively established in the present study and the study [6].

Figure 16 illustrates the positions of neutral layer under different local loading pattern. As declared in the study [6], with the increase in the stroke (s) and the width (l) of local

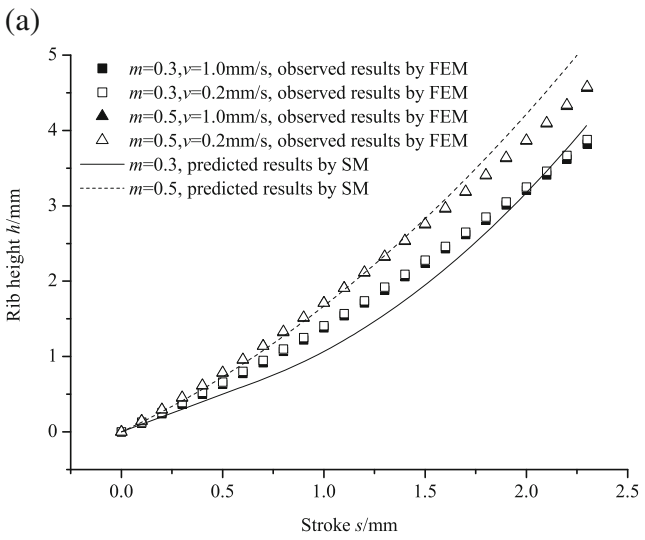

Fig. 14 Rib height under different forming conditions: **a** Ti-6Al-4 V, T =950 °C; **b** TA15, T=970 °C

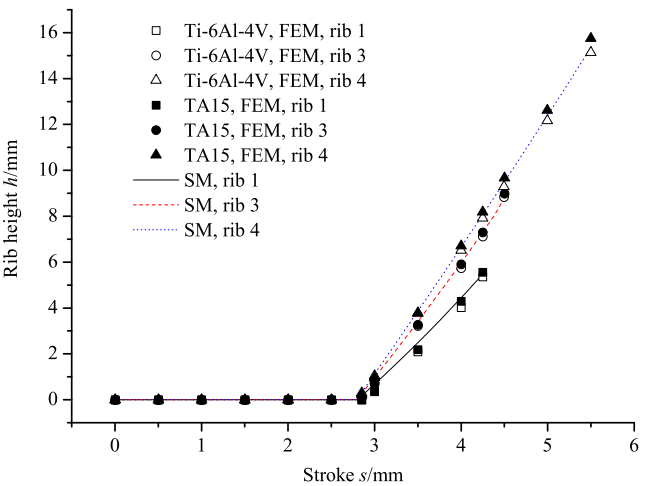

Fig. 15 Rib heights of rib 1, 3 and 4 in local loading state

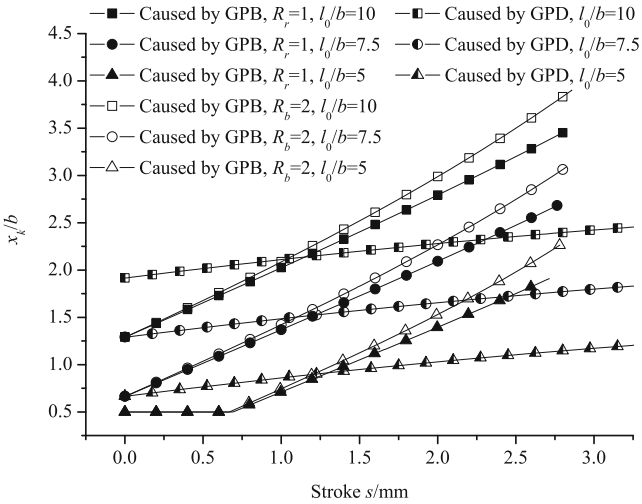

Fig. 16 Positions of neutral layer under different local loading patterns

loading, the position (x_k) of neutral layer keeps away from the center of rib cavity. The value of x_k under local loading pattern caused by GPB is less than that under the pattern caused by GPD at initial forming stage. However, the x_k under local loading pattern caused by GPB increases quickly with the increase in s, and then the value becomes much greater than that under local loading pattern caused by GPD. The main reason for this phenomenon is that the l dynamically changes and increases quickly with the increase in s under the local loading pattern caused by GPB. The increasing speed of l under beveling pattern is greater than that under rounding pattern, so the x_k under beveling pattern is larger than that under rounding pattern gradually.

The rib height h is determined by the position of neutral layer. The change of rib height is similar to that of the x_k, as shown in Fig. 17. However, under different local loading patterns, the change in x_k is more notable than that in rib

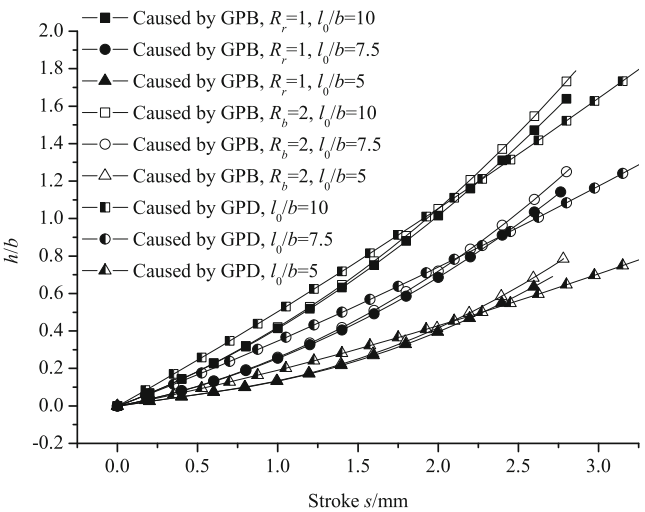

Fig. 17 Rib heights under different local loading patterns

height because h is an accumulated value while x_k is not. The metal flowing into rib cavity under local loading pattern caused by GPB is less than that under the pattern caused by GPD at initial forming stage, so the rib height under the local loading pattern caused by GPB is also less than that under local loading pattern caused by GPD. With the increase in stroke, the increasing speed of x_k under the local loading pattern caused by GPB greater than that under local loading pattern caused by GPD, and then the metal flowing into rib cavity under local loading pattern caused by GPB is greater than that under local loading pattern caused by GPD gradually. So the difference of rib height between the local loading patterns caused by GPB and caused by GPD will reduce and the rib height under the local loading pattern caused by GPB may be greater than rib height under the local loading pattern caused by GPD.

During local loading forming, there exist shearing deformation and upsetting-extruding deformation depending on the geometric parameters of die and billet. Figure 18 illustrates the deformation patterns under different geometric parameters according to the transition conditions between shearing deformation and upsetting-extruding deformation in the SM models. The time of shearing deformation in the process reduces with increasing l_0 and decreasing H_0. But for local loading pattern caused by GPB, the range of initial parameters making rib cavity be filled under upsetting-extruding deformation throughout the forming process is smaller than that for local loading pattern caused by GPD. It can be seen from Fig. 16 that whenl_0/b=5, the deformation pattern is upsetting-extruding deformation under local loading pattern caused by GPD throughout the forming process but shearing deformation occurs at initial forming stage for local loading pattern caused by GPB. In order to make upsetting-extruding deformation occurs throughout the forming process (l_0/b=5under local loading pattern caused by GPB), $\Delta H_0/H_0$should reduce to less than 0.36 or l_0/b increases up to greater than 6.83, but it may be difficult to achieve initial metal distribution. Fortunately, l will increase quickly and shearing deformation will turn into upsetting-extruding quickly. The metal flowing outward is only to achieve second metal distribution but not to cause defects about flow line for neighbor rib. The initial parameters for local loading pattern caused by GPB may be selected according to the Fig. 18a.

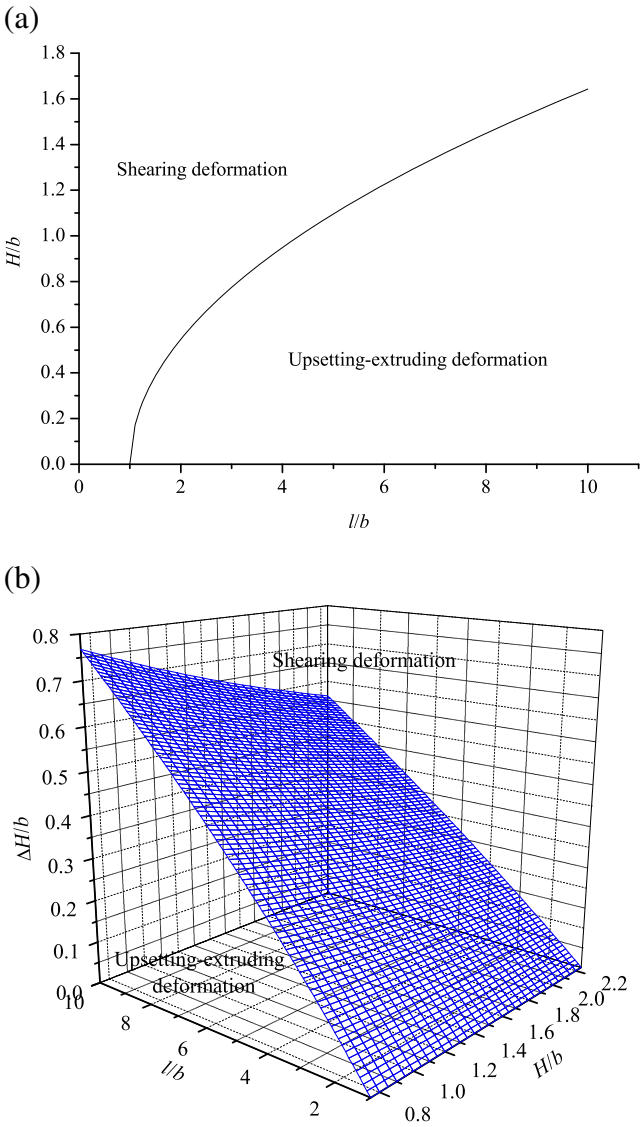

Fig. 18 Effects of geometrical parameters on deformation pattern under different local loading patterns: **a** local loading pattern caused by GPD; **b** local loading pattern caused by GPB

6 Conclusions

(1) A SM model for local loading pattern caused by GPB is established by introducing new assumptions, variables and boundary conditions. A predicted model for the dynamic width of local loading is established by using polynomial regression and PLS regression, which provides the dynamic width l under different initial geometric parameters for SM model. The models can be used to analyze the rib-web component isothermal local loading process of Ti-6Al-4 V and TA15 titanium alloy under loading speed v=0.1–1.0 mm/s and forming temperature 950–970 °C. The comparison between the predicted results by regression model and the FEM results indicates that the error of predicted model for the dynamic width is less than about 10 %. Comparing with FEM and physical modeling experimental results indicates that the error of SM model for rib height is less than about 15 %.

(2) The metal flow and deformation pattern under local loading are determined by the thickness of billet and the width of local loading. The deformation pattern for

the local loading patterns caused by GPD and GPB are the same, there exist shearing deformation and upsetting-extruding deformation. During local loading forming process, the changes of the thickness of billet and the width of local loading are different for different local loading patterns, and the changes of the position of neutral layer are also different, and thus transition conditions between two deformation patterns are different.

(3) When the initial geometric parameters are the same, the value of x_k (position of neutral layer) under local loading pattern caused by GPB is less than that under local loading pattern caused by GPD at initial forming stage, but the increasing speed of the position of neutral layer for the former is greater than that for the latter. The range of parameters to avoid shearing deformation under local loading pattern caused by GPB is smaller than that for the pattern caused by GPD at initial forming stage, but the shearing deformation under the pattern caused by GPB will turn into upsetting-extruding deformation quickly.

Acknowledgments The authors would like to gratefully acknowledge the supports of National Natural Science Foundation of China for key program (Grant No. 50935007), National Basic Research Program of China (973 Program, Grant No. 2010CB731701), and the 111 Program (Grant No. B08040).

Appendix A. Abbreviations

ETB	Equal-Thickness Billet
FEA	Finite Element Analysis
FEM	Finite Element Method
GPB	Geometric Parameters of Billet
GPD	Geometric Parameters of Die
PLS	Partial Least Squares
SM	Slab Method
UTB	Unequal-Thickness Billet
VTRB	Variable-Thickness Region of Billet

References

1. Leyens C, Peters M (2003) Titanium and titanium alloys. Wiley-VCH, Weinheim
2. Yang H, Fan XG, Sun ZC, Guo LG, Zhan M (2011) Recent developments in plastic forming technology of titanium alloys. Sci China Tech Sci 54:490–501
3. Shan D, Xu W, Si C, Lu Y (2007) Research on local loading method for an aluminium-alloy hatch with cross ribs and thin webs. J Mater Process Technol 187–188:480–485
4. Sun ZC, Yang H (2008) Mechanism of unequal deformation during large-scale complex integral component isothermal local loading forming. Steel Res Int 79(Special Edition 1):601–608
5. Sarkisian JM, Palitsch JR, Zecco JJ (1999) Stepped, segmented, closed-die forging, United States Patent, Patent Number: 5950481
6. Zhang DW, Yang H, Sun ZC (2010) Analysis of local loading forming for titanium-alloy T-shaped components using slab method. J Mater Process Technol 210:258–266
7. Altan T, et al. (1982) Modern Forging: Equipment, Materials and Process, S. Lu, translated, Defence Industrial Press, Beijing (in Chinese)
8. Kong TF, Chan LC, Lee TC (2008) Numerical and experiment investigation perform design in non-axisymmetric warm forming. Int J Adv Manuf Technol 37:908–919
9. Zhang DW, Yang H, Sun ZC, Fan XG (2010) A New FE Modeling Method for Isothermal Local Loading Process of Large-scale Complex Titanium Alloy Components Based on DEFORM-3D. In: Barlat F, Moon YH, Lee M-G (eds) AIP Conference Proceedings 1252. American Institute of Physics, Melville, New York, pp 439–446
10. Sun NG, Yang H, Sun ZC (2009) Optimization on the process of large titanium bulkhead isothermal closed-die forging. Rare Metal Mat Eng 38(7):1296–1300 (in Chinese)
11. Sun ZC, Yang H (2009) Forming quality of titanium alloy large-scale integral components isothermal local loading. Arab J Sci Eng 34(1C):35–45
12. Park JJ, Hwang HS (2007) Preform design for precision forging of an asymmetric rib-web type component. J Mater Process Technol 187–188:595–599
13. Zhang DW, Yang H, Sun ZC, Fan XG (2012) Deformation behavior of variable-thickness region of billet in rib-web component isothermal local loading process. Int J Adv Manuf Technol 63:1–12
14. Altan T, Fiorentino RJ (1971) Prediction of loads and stresses in closed-die forging. J Eng Ind Trans ASME Ser B 93:477–484
15. Chitkara NR, Aleem A (2001) Extrusion of axi-symmetric tubes from hollow and solid circular billet: a generalised slab method of analysis and some experiments. Int J Mech Sci 43:1661–1684
16. Qwamizadeh M, Kadkhodaei M, Salimi M (2012) Asymmetrical sheet rolling analysis and evaluation of developed curvature. Int J Adv Manuf Technol 61:227–235
17. Altan T, Oh SI, Gegel HL (1983) Metal forming: fundamentals and application. American Society for Metals, Metal Park, OH
18. Boër CR, Rebelo N, Rydstad H, Schröder G (1986) Process modelling of metal forming and thermomechanical treatment. Springer, Berlin
19. O'Connell M, Painter B, Maul G, Altan T (1996) Flashless closed-die upset forging-load estimation for optimal cold header selection. J Mater Process Technol 59:81–94
20. Wold S, Sjöström M, Eriksson L (2001) PLS-regression: a basic tool of chemometrics. Chemom Intell Lab Syst 58:109–130
21. Wold S, Martens H, Wold H (1983) The multivariate calibration problem in chemistry solved by the PLS method. Lecture Notes in Mathematics 97:286–293
22. Zhang DW, Yang H, Li HW, Fan XG (2012) Friction factor evaluation by FEM and experiment for TA15 titanium alloy in isothermal forming process. Int J Adv Manuf Technol 60:527–536